An Empirical Model of Ionospheric Field-Aligned Currents as a Function of the Interplanetary Magnetic Field

D. R. Weimer
Mission Research Corp.
Nashua, NH

Abstract. A new technique for mapping field-aligned currents with satellite magnetometer data has been used with Dynamics Explorer 2 measurements to produce an empirical model which maps the currents above the high-latitude ionosphere as a function of the IMF, solar wind velocity, solar wind density, and dipole tilt angle. This technique uses scalar magnetic Euler potentials, derived from integrating the measured magnetic deviations in much the same way as electric potentials are derived from integrating electric fields. This method works with any configuration of two-dimensional distribution of the field-aligned current, rather than assuming that the currents are in the form of infinite sheets or belts. The radial current density is found by a surface Laplacian operator on the scalar field. The maps of the FAC produced with this new technique are more quantitative and detailed than most of the preceding statistical diagrams, and they yield much insight into how the currents vary as the IMF clock angle changes, and how the field-aligned current maps overlap the associated electric potential patterns. An optional component of the model shows changes in the currents associated with substorms, using the *AL* index as the controlling parameter. The most notable aspect of the substorm patterns is an increased region 0

current, which in addition to the region 2 current closes the majority of the current on the dusk side of the auroral surge.

A New Technique For Deriving Currents From Magnetometer Data

In the past nearly all measurements of field-aligned current density using satellite magnetometer data have relied upon the "infinite current sheet approximation." Precise determination of the currents is not possible with one satellite magnetometer measurement; in order to eliminate the geometry assumptions it is necessary to construct a two-dimensional map of the magnetic perturbation. A new technique introduced by *Weimer* [2000a] and finalized in *Weimer* [2000c] constructs statistical maps from multiple satellite passes using a scalar magnetic Euler potential, which is then used to derive the distribution of field-aligned currents on a surface. A brief summary of the technique is given here (many equations can be found in *Backus* [1986]). Start with a curvilinear coordinate system having orthogonal unit tangent vectors $\mathbf{e_1}$, $\mathbf{e_2}$, and $\mathbf{e_3}$, and a current that is only in one direction, such as $\mathbf{e_1}$:

$$\mathbf{J} = J\,\mathbf{e_1} \quad . \tag{1}$$

If $\mathbf{e_1}$ is in the radial direction in a spherical coordinate system, or any direction in a Cartesian system, then magnetic field on the orthogonal surface is such that

$$\Delta\mathbf{B} = \mathbf{e_1} \times \nabla_S \psi \quad . \tag{2}$$

∇_S is the "surface gradient" in the $\mathbf{e_2}$ and $\mathbf{e_3}$ directions, and ψ is a "scalar magnetic potential." This potential can also be considered to be the same as one of two "Euler potential," as described by *Stern*

[1970], where the other potential is constant on the surface. The current and associated magnetic field perturbations are related by

$$\mu_o \mathbf{J} = \nabla \times \Delta \mathbf{B} = \nabla \times (\mathbf{e_1} \times \nabla_S \psi) \quad . \tag{3}$$

It follows that the current density is related to the scalar magnetic potential by

$$\mu_o J = \nabla_S^2 \psi \quad , \tag{4}$$

where ∇_S^2 is the two-dimensional "surface Laplacian." As (2) can be rewritten as

$$\mathbf{e}_1 \times \Delta \mathbf{B} = -\nabla_S \psi \tag{5}$$

then the potential ψ can be obtained by integrating $\mathbf{e}_1 \times \Delta \mathbf{B}$. This is analogous to the case of an electric potential, where the electric field is defined as

$$\mathbf{E} = -\nabla_S \Phi \tag{6}$$

and the potential is obtained from measurements of electric fields by an integration along the path of measurement.

To apply these equations to the processing of satellite magnetometer data, the measured magnetic field first has the geomagnetic field subtracted, using the DGRF reference model, and the resulting delta-B is then crossed with a vector in the upward direction. Next, the component of the resulting vector that is in the direction of motion is integrated to obtain the scalar magnetic potential along the path. An example is shown in **Figure 1**. After using many satellite passes to derive a statistical map of the magnetic potential on the entire two-dimensional spherical surface, the field-aligned currents are then derived with a spherical surface Laplacian operation:

$$\nabla_S^2 \psi = \frac{1}{r^2 \sin\theta} \frac{\partial}{\partial \theta} \left(\sin\theta \frac{\partial \psi}{\partial \theta} \right) + \frac{1}{r^2 \sin^2 \theta} \frac{\partial^2 \psi}{\partial \varphi^2} \quad . \tag{7}$$

The above equations are easily verified in Cartesian coordinates. In spherical coordinates this theory is less intuitive, but it is known that the total magnetic field in a spherical shell can be separated into "poloidal" and "toroidal" vector fields. The $\Delta\mathbf{B}$ in (2) is the toroidal field and ψ is the toroidal scalar for **B.** "The toroidal magnetic field comes entirely from the poloidal current" and "the poloidal current is also the radial component of the total current" [*Backus*, 1986, p. 93]. Thus the one and only limiting assumption with this technique is that it only measures the radial current, rather than that precisely parallel to the dipole field lines.

Use with DE-2 Data

The Dynamics Explorer-2 satellite operated between August 1981 and March 1983, taking measurements with a variety of instruments in a polar orbit at altitudes of 300 to 1000 km. There has not been a similarly equipped, low-altitude, polar orbiting science mission flown by NASA in the 20 years since then, so the DE-2 data have remained a valuable and unsurpassed asset. The electric field measurements had already been found to be useful for building statistical models of the polar electric potentials [*Weimer*, 1995, 1996, 2000b], so it is logical to use the magnetic field measurements from DE-2 [*Farthing et al.*, 1981] to build a comparable statistical model of the magnetic field-aligned currents, obtained under identical conditions. (Yes, now that Oersted has been launched, better magnetic field data are becoming available.)

There were found to be 2438 passes with good magnetometer data. The magnetometer data from each pass was processed through

the sequence of steps shown in **Figure 1**. The latitude and magnetic local time (MLT) in Altitude Adjusted Corrected Geomagnetic Coordinates (AACGM) was computed for every point of measurement. In essence, this procedure maps the potentials along field lines, treating the magnetic field lines as if they were equipotentials. As the potential distribution is defined as a function of latitude and longitude (MLT) on the surface of a sphere, (4) can be used to calculate the radial current distribution on that sphere.

After computing the magnetic potential for all passes in the data base, maps of the magnetic potential in two dimensions on the surface of a sphere are generated for specific groupings, according to IMF/solar wind conditions, by fitting the data with spherical harmonics. The data points were stretched in colatitude so that they spanned the entire range from 0 to $\pi/2$, thus reducing the order of the spherical harmonics that are required to fit the data. The low-latitude boundary that determined the stretching function was an offset oval, represented with a second-order Fourier series function of MLT. From a number of maps derived for a variety of conditions it is possible to determine how the spherical harmonic coefficients, which define a potential map, vary as a function of the IMF magnitude and orientation, the solar wind velocity and density, and the dipole tilt angle (which depends on the day of year and time of day). A process was used that is identical to that which was used for the electric potential model, as described in more detail by *Weimer* [1996, 2000b].

The end result is a table of regression and Fourier coefficients which can recreate the spherical harmonic coefficients for any arbitrary IMF/solar wind conditions and reproduce the scalar magnetic potential distribution, which is then used to calculate the field-aligned currents by means of Equations (4) and (7). Using the

spherical harmonic expression for the potential ψ, the result is a series of associated Legendre polynomials and their first derivatives (the latitude stretching factor is taken into consideration). One example of the magnetic potential and the derived field-aligned current is shown in **Figure 2.**

Results From the FAC Model

Maps of the magnetic field-aligned current as a function of corrected geomagnetic latitude (CGLAT) and magnetic local time (MLT) are shown in **Figure 3** for eight equally spaced orientations of the IMF "clock angle" in the GSM *Y-Z* plane, having a fixed magnitude of 5 nT in that plane. The solar wind velocity for this example is 400 km-s^{-1}, the number density is 5 cm^{-3}, and the dipole tilt angle is zero. The current density is evaluated at a radial distance corresponding to an altitude of 115 km. The sign convention is such that positive currents are downward and negative currents are upward. On each map the location of the largest positive current is indicated with a plus sign, and the location of the most negative current is indicated with a diamond symbol. The values of these peaks are indicated in the lower left and right corners of each diagram. It is emphasized that these are maps of the average FAC distribution, consistent with the large-scale magnetic perturbations. In reality the currents have an embedded, small-scale structure where the current density greatly exceeds the average values.

For a southward-directed IMF in the -Z direction the conventional region 1 and 2 belts are plainly visible in the **Figure 3** diagram, although in this quantified graph they appear much thicker than in the historical current sheet diagrams. For an IMF in the +Z direction the map shows a clear "NBZ" current system surrounded by the region 1 and 2 currents. This NBZ system consists of a pair of

“region 0" currents that have a polarity opposite to the surrounding region 1 currents. As these region 0 currents are cylindrically shaped, the use of the infinite current sheet approximation can be problematic when the IMF is northward. It is noteworthy that this same geometry can be reproduced with an MHD simulation of the magnetosphere with a northward IMF, as shown in the example in Plate 5 by *Siscoe et al.* [2000].

For IMF in the +Y direction the upward region 1 current that is on the dusk side wraps through noon to become the region 0 current on the dawn side. The downward region 1 current on the dawn side continues into the region 2 current on the dusk side. Again there are similarities to MHD simulations, as in Plate 8 by *Siscoe et al.* [2000]. The upward region 0-1 current encircles a small area of downward current, which appears to be a remnant of the other region 0 pair in the NBZ system. Note that these maps show a logical, consistent, and orderly evolution of the current systems as the IMF rotates around the circle

The result of doubling the magnitude of the IMF is shown in the maps in **Figure 4**. The effects of the stronger IMF are most pronounced with the region 0 or NBZ currents. In order to study the effects of the dipole tilt angle, or season, **Figure 5** shows results with the same conditions as in Figure 1 except for at tilt angle corresponding to the winter solstice in the northern hemisphere, and **Figure 6** uses a tilt angle for the summer solstice (during each day the actual tilt varies by about ±11° from these values). The winter patterns are weaker and disorganized, almost to the point of appearing random. The summer patterns, as expected, have much stronger current magnitudes, and again the NBZ system is very prominent.

The validity of this flexible FAC model can be demonstrated by a comparison with the magnetometer data from a few individual

orbits. **Figure 7** shows two examples. The field-aligned currents are represented by the color shading, as indicated with the scale on the left. Contour lines of the magnetic Euler potentials that are generated by the model, and used to calculate the same currents, are superimposed on this graph. The contour levels are marked on the right, in units of centitesla-meters (cTm). The magnetic field perturbations that were measured with the magnetometer on DE-2 (geomagnetic field subtracted) are shown along the path of the spacecraft with the vector lines. It is a well-known property of Euler potentials, and it follows from Equation (5), that the equipotential lines are in the same direction as the magnetic field lines, with a magnitude proportional to the gradient between potentials. Given this, there is an excellent agreement between the measured perturbation vectors and the underlying contour lines. Incidentally, these contour lines also indicate the direction of the stress applied to the ionosphere by the magnetosphere, as shown by *Iijima* [2000] and *Strangeway et al.* [2000].

As there have been longstanding, fundamental questions about the relationships between the field-aligned currents and electric potential patterns, it is very informative to superimpose the results of the FAC model with the newest electric potential model [*Weimer*, 2000b]. **Figure 8** shows two examples, one with the IMF in the negative *Y* direction (**Figure 8a**), and the other in the positive *Y* direction (**Figure 8b**). Both used an IMF magnitude of 8 nT, and the format is nearly the same as in Figure 7, with the electric potential replacing the magnetic potential. These pictures show an excellent agreement with the conceptual diagrams presented by *Cowley et al.* [1991].

Total Currents

The sum of all current into the hemisphere has been computed with the FAC model for a number of IMF conditions and compared with the electric potential that is generated for the same conditions with the twin model. The sum of the outward current was also computed, and it was found to have magnitudes agreeing very well with the inward current, usually with a difference of less than 1% of the total, the disparity attributable to the finite precision of the numerical integration. **Figure 9a** shows the results of varying the IMF magnitude from 1 to 15 nT, in 1 nT steps, at clock angles of -90°, +90°, and 180°, and varying from 6 nT to 15 nT for a purely northward IMF, under which conditions there was a well-established pair of reversed potential cells. An additional line shows the results of varying the IMF clock angle from 60° to 300°, with the magnitude fixed at 8 nT. A tilt angle of zero was used, so these currents are for equinox conditions.

Figure 9b shows the net total of all current on the dawn side, at 0 to 1200 MLT, for the same cases as in Figure 9a. This sum is the amount of the region 1 current that is not closed with the region 0 and region 2 current on the dawn side, and therefore must cross the polar cap and close through an equally unbalanced region 1 current on the dusk side, with an opposite net sign. In most cases 20% of the region 1 current crosses the polar cap over the noon-midnight line, and 80% closes on the same side. The slope of the lines in **Figure 9b** is an indication of the net conductance across the polar cap. It is not always a precise measurement, since at some clock angles the region 1 current passes through the 1200 MLT meridian to become the region 0 current on the opposite side, thereby reducing the magnitude of integrated totals on each side. The curve in the graph representing the variable clock angle, which makes a loop rather than line, shows the effects of the region 1 rotating as the clock angle changes.

For the line representing the 0° clock angle case, the total dawn current was actually negative (absolute value shown) and the electric potential was negative, with the locations of the peak potentials reversed between dawn and dusk. The currents which cross the dawn-dusk boundary are due to the region 0, NBZ currents. The conductance for the northward IMF is higher since the closure path of the NBZ currents through the ionosphere is much shorter than that for region 1 currents.

Substorm Currents

When the electric potential measurements from the satellite passes are sorted according to whether or not substorm are present, the patterns show distinct changes with substorms. The revised electric potential model [*Weimer*, 2000b] incorporated these substorm patterns, along with others derived by sorting passes on just the magnitude of the lower Auroral Electrojet index, *AL*, to produce a "substorm module" in the potential model. This optional component is controlled by the *AL* index, and it operates as a perturbation to the underlying pattern in order to model the nightside processes that are more independent of the IMF. As the FAC model is constructed from the same program, it too includes the optional component.

Figure 10 shows the FAC patterns resulting from use of the optional perturbation module, varying the *AL* index from 0 to -1200 nT in -150 nT steps, with the other parameters fixed with an IMF clock angle of +90°. The results show that with increasing the absolute magnitude of the *AL* index there is an increase in the upward, region 1 current near 2100 MLT. This upward current would appear to be part of a "substorm current wedge," but the corresponding part of the wedge system in the downward current on the dawn side was simply not present in the magnetometer data. Instead, there grew a

region of downward current poleward of the upward current on the dusk side at 2100 MLT. This downward current could be classified as a region 0, and there also grew an upward region 0 current on the dawn side. Summation of the currents in these maps indicates that, while the total of all currents, including region 2, increases significantly as the *AL* index increases in magnitude, the region 0 current has the proportionally largest increase. The net sum of all current on the dusk side, on the other hand, does not increase much in proportion to the others. In fact, for some other IMF angles the net dusk and dawn currents stay steady or even decrease as the magnitude of *AL* increases, due to the effects of more current being closed through region 0 or a rotation of the patterns through the dawn-dusk meridian.

Summary

A new technique for mapping field-aligned currents with satellite magnetometer data has been used to produce an empirical model that can produce maps of the currents above the high-latitude ionosphere as a function of the IMF, solar wind velocity, solar wind density, and dipole tilt angle. This technique uses scalar magnetic Euler potentials, derived from integrating the measured magnetic deviations in much the same way as electric potentials are derived from integrating electric fields. The radial current density is found by a surface Laplacian operator on the scalar field. The FAC maps produced with this method do not assume a sheet-like geometry.

Previous statistical models of the FAC typically show just qualitative outlines of regions of upward and downward currents, usually as belts, for just a few general IMF conditions [i.e., *Iijima and Potemra*, 1976]. The maps of the FAC produced with this new technique are much more quantitative, show details not previously

available, and yield much insight into how the currents vary as the IMF clock angle changes. It is also useful to see how the field-aligned current maps overlap the associated electric potential patterns. Total currents are similar to those obtained by other methods.

This FAC model can also use the *AL* index as an optional parameter, showing changes in the currents associated with substorms. The most notable aspect of the substorm patterns is the increased region 0 current, which in addition to the region 2 current closes the majority of the current on the dusk side of the auroral surge.

Acknowledgments. This research was supported by NSF grants ATM-9701868 and ATM-9727554. The author thanks Nelson Maynard for helpful comments. The data from DE-2, IMP-8, and ISEE 3 were provided on CD-ROM by the National Space Science Data Center. Masahisa Sugiura and Jim Slavin are Principal Investigators for the magnetometer on DE-2. Ron Lepping and Alan Lazarus are the Principal Investigators for the magnetometer and plasma instruments on IMP-8. Edward Smith and John Gosling are the Principal Investigators for the magnetometer and plasma instruments on ISEE-3.

References

Backus, G., Poloidal and toroidal fields in geomagnetic field modeling, *Rev. Geophys., 24*, 75, 1986.

Cowley, S. W. H., J. P. Morelli, and M. Lockwood, Dependence of convective flows and particle precipitation in the high-latitude dayside ionosphere on the X and Y components of the interplanetary magnetic field, *J. Geophys. Res., 96*, 5557, 1991.

Farthing, W. H., M. Sugiura, B. G. Ledley, and L. J. Cahill, Jr.,

Magnetic field observations on DE-A and -B, *Space Sci. Instrum., 5,* 551-560, 1981.

Iijima, T. and T. A. Potemra, Large-scale characteristics of field-aligned currents associated with substorms, *J. Geophys. Res., 81*, 3999, 1976.

Iijima, T., Field-aligned currents in geospace: substance and significance, in *Magnetospheric Current Systems, Geophys. Monogr. Ser.*, vol. 118, edited by S. Ohtani, R. Fujii, M. Hesse, and R. L. Lysak, AGU, Washington, D. C., pp. 107-129, 2000.

Siscoe, G. L, N. U. Crooker, G. M. Erickson, B. U. Ö. Sonnerup, K. D. Siebert, D. R. Weimer, W. W. White, N. C. Maynard, Global geometry of magnetospheric currents inferred from MHD simulations, in *Magnetospheric Current Systems, Geophys. Monogr. Ser.*, vol. 118, edited by S. Ohtani, R. Fujii, M. Hesse, and R. L. Lysak, AGU, Washington, D. C., pp. 41-52, 2000.

Stern, D. P., Euler potentials, *Am. J. Phys., 38*, 494, 1970.

Strangeway, R. J., R. C. Elphic, W. J. Peria, and C. W. Carlson, FAST observations of electromagnetic stresses applied to the polar ionosphere, in *Magnetospheric Current Systems, Geophys. Monogr. Ser.*, vol. 118, edited by S. Ohtani, R. Fujii, M. Hesse, and R. L. Lysak, AGU, Washington, D. C., pp. 21-29, 2000.

Weimer, D. R., Models of high-latitude electric potentials derived with a least error fit of spherical harmonic coefficients, *J. Geophys. Res., 100*, 19,595, 1995.

Weimer, D. R., A flexible IMF dependent model of high-latitude electric potentials having "space weather" applications, *Geophys. Res. Lett., 23*, 2549, 1996.

Weimer, D. R., Substorm influence on the ionospheric electric potentials and currents, *J. Geophys. Res., 104*, 185, 1999.

Weimer, D. R., A new technique for the mapping of ionospheric

field-aligned currents from satellite magnetometer data, in *Magnetospheric Current Systems*, *Geophys. Monogr. Ser.*, vol. 118, edited by S. Ohtani, R. Fujii, M. Hesse, and R. L. Lysak, AGU, Washington, D. C., pp. 381-388, 2000a.

Weimer, D. R., An improved model of ionospheric electric potentials including substorm perturbations and application to the GEM November 24, 1996 event, *J. Geophys. Res.*, in press, 2000b.

Weimer, D. R., Maps of Ionospheric Field-Aligned Currents as a Function of the Interplanetary Magnetic Field Derived From Dynamics Explorer 2 Data, *J. Geophys. Res.*, in press, 2000c.

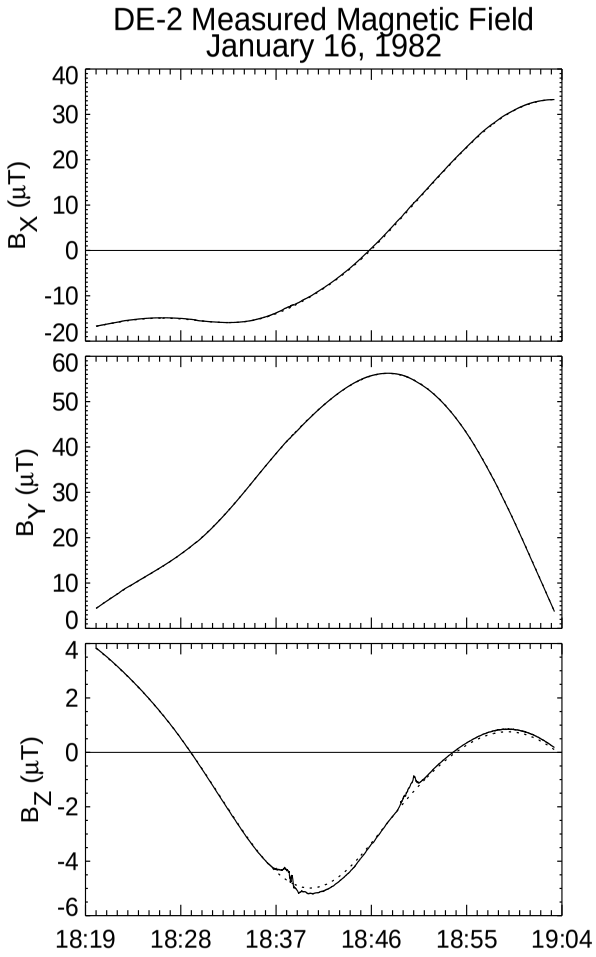
DE-2 Measured Magnetic Field
January 16, 1982
B_X (μT)
B_Y (μT)
B_Z (μT)
18:19
18:28
18:37
18:46
18:55
19:04

A

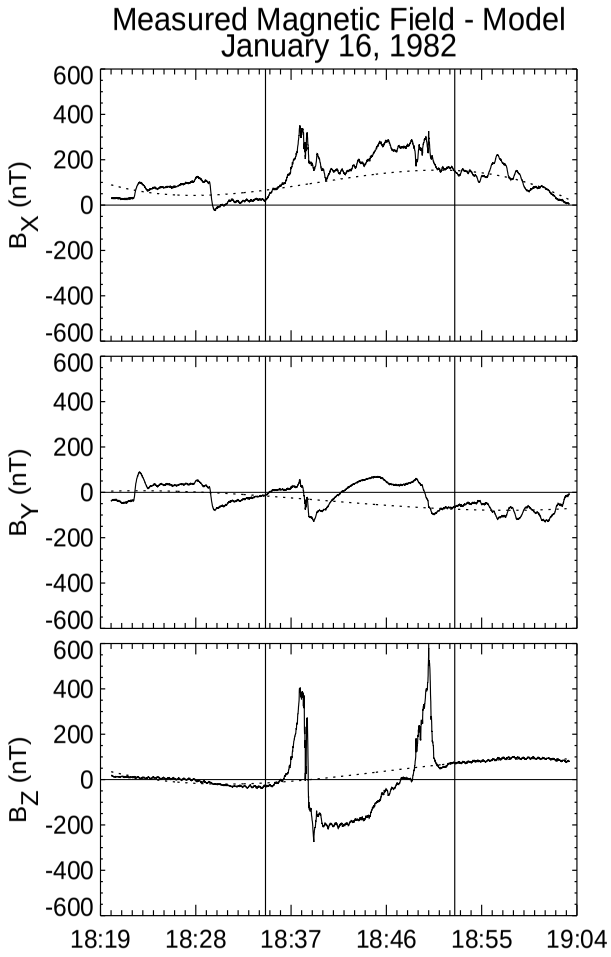
Measured Magnetic Field - Model
January 16, 1982
B_X (nT)
B_Y (nT)
B_Z (nT)
18:19
18:28
18:37
18:46
18:55
19:04

B

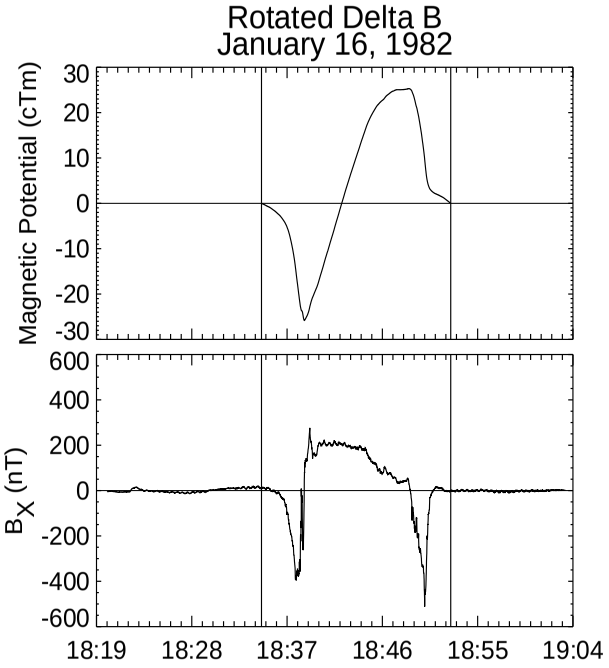
Rotated Delta B
January 16, 1982
Magnetic Potential (cTm)
B_X (nT)
18:19
18:28
18:37
18:46
18:55
19:04

C

Figure 1

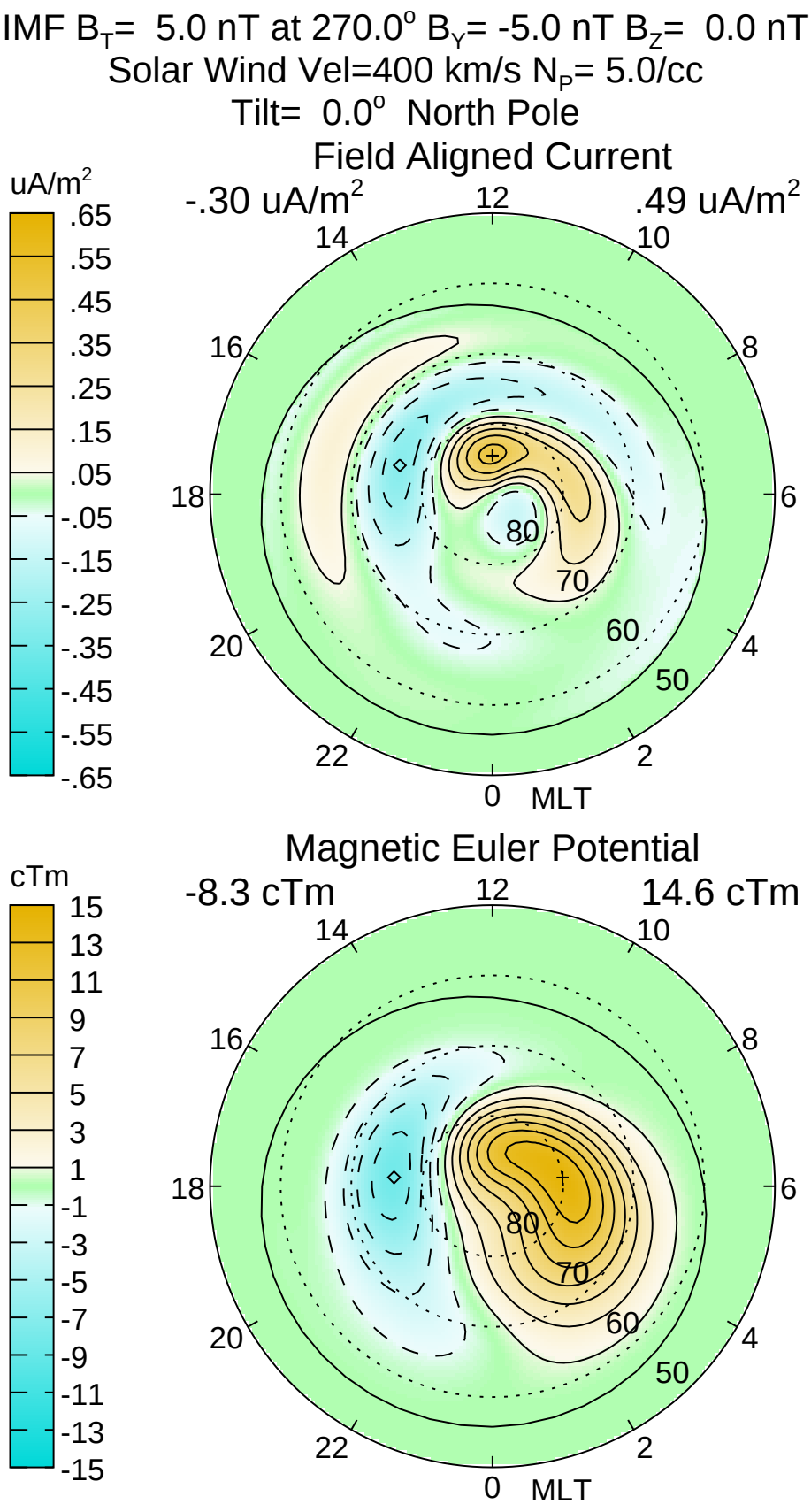
IMF B_T= 5.0 nT at 270.0° B_Y= -5.0 nT B_Z= 0.0 nT
Solar Wind Vel=400 km/s N_P= 5.0/cc
Tilt= 0.0° North Pole
Field Aligned Current
uA/m²
.65
.55
.45
.35
.25
.15
.05
-.05
-.15
-.25
-.35
-.45
-.55
-.65
-.30 uA/m²
.49 uA/m²
12
14
10
16
8
18
6
20
4
22
2
0 MLT
80
70
60
50
Magnetic Euler Potential
cTm
15
13
11
9
7
5
3
1
-1
-3
-5
-7
-9
-11
-13
-15
-8.3 cTm
14.6 cTm
12
14
10
16
8
18
6
20
4
22
2
0 MLT
80
70
60
50

Figure 2

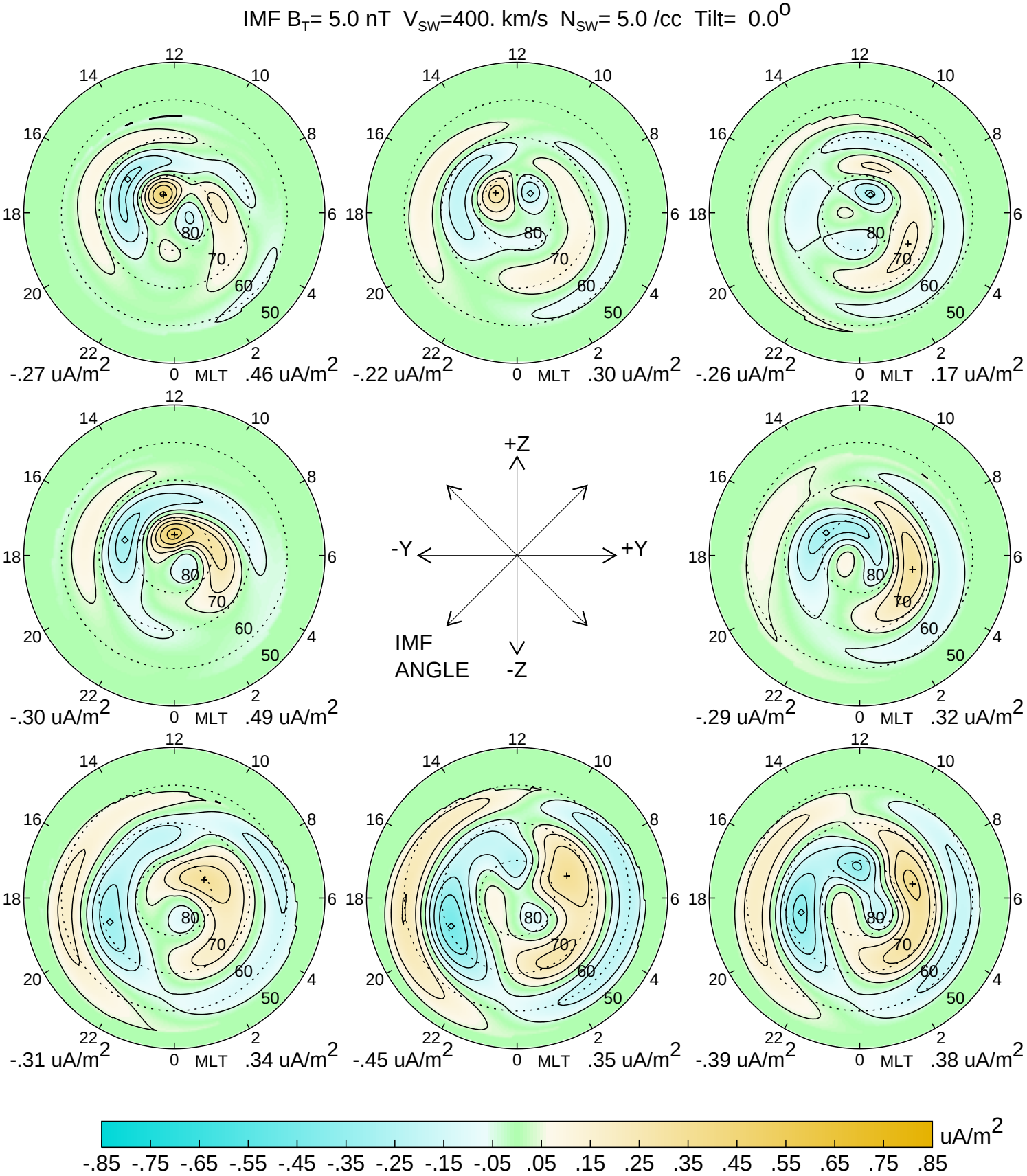
Field Aligned Current
IMF B_T= 5.0 nT V_{SW}=400. km/s N_{SW}= 5.0 /cc Tilt= 0.0°
-.27 uA/m2
.46 uA/m2
-.22 uA/m2
.30 uA/m2
-.26 uA/m2
.17 uA/m2
-.30 uA/m2
.49 uA/m2
+Z
-Y
+Y
IMF
ANGLE
-Z
-.29 uA/m2
.32 uA/m2
-.31 uA/m2
.34 uA/m2
-.45 uA/m2
.35 uA/m2
-.39 uA/m2
.38 uA/m2
MLT
uA/m2
-.85 -.75 -.65 -.55 -.45 -.35 -.25 -.15 -.05 .05 .15 .25 .35 .45 .55 .65 .75 .85

Figure 3

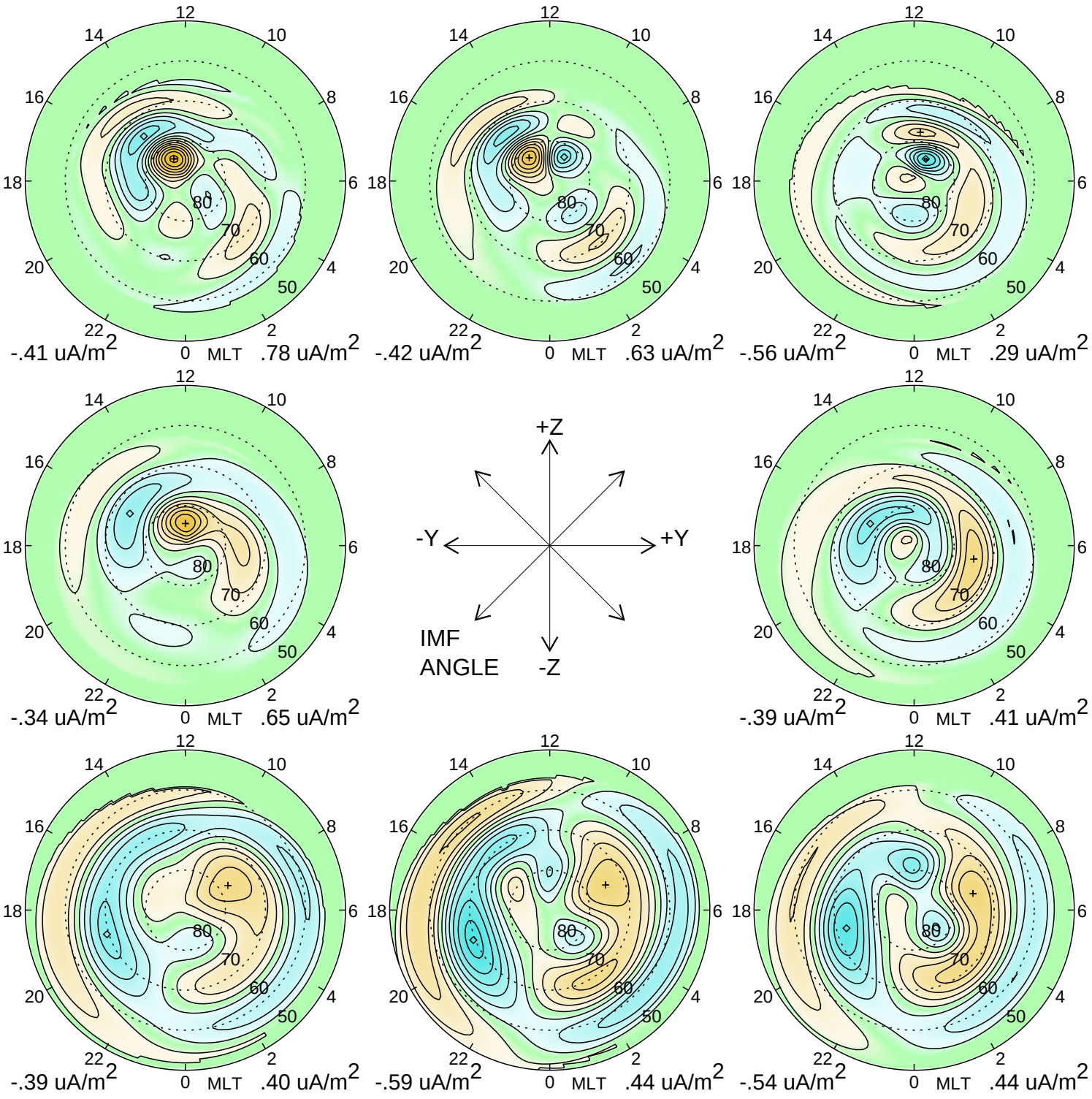
Field Aligned Current
IMF B_T=10.0 nT V_{SW}=400. km/s N_{SW}= 5.0 /cc Tilt= 0.0^o
-.41 uA/m^2
.78 uA/m^2
-.42 uA/m^2
.63 uA/m^2
-.56 uA/m^2
.29 uA/m^2
-.34 uA/m^2
.65 uA/m^2
+Z
-Y
+Y
IMF
ANGLE
-Z
-.39 uA/m^2
.41 uA/m^2
-.39 uA/m^2
.40 uA/m^2
-.59 uA/m^2
.44 uA/m^2
-.54 uA/m^2
.44 uA/m^2
MLT
uA/m^2
-.85 -.75 -.65 -.55 -.45 -.35 -.25 -.15 -.05 .05 .15 .25 .35 .45 .55 .65 .75 .85

Figure 4

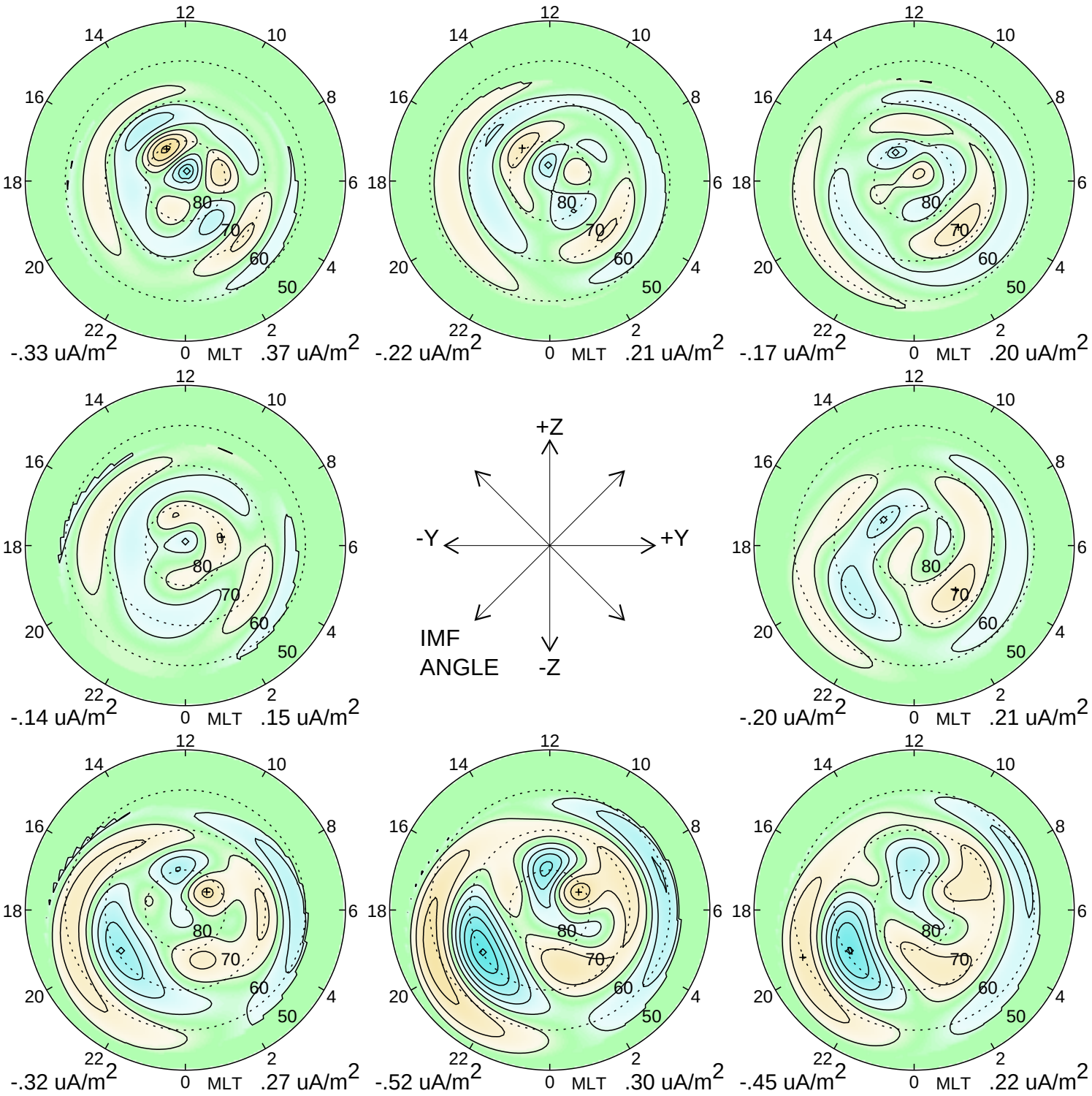
Field Aligned Current
IMF B_T= 5.0 nT V_{SW}=400. km/s N_{SW}= 5.0 /cc Tilt=-23.4^o
-.33 uA/m^2
.37 uA/m^2
-.22 uA/m^2
.21 uA/m^2
-.17 uA/m^2
.20 uA/m^2
-.14 uA/m^2
.15 uA/m^2
+Z
-Y
+Y
IMF
ANGLE
-Z
-.20 uA/m^2
.21 uA/m^2
-.32 uA/m^2
.27 uA/m^2
-.52 uA/m^2
.30 uA/m^2
-.45 uA/m^2
.22 uA/m^2
MLT
uA/m^2
-.85 -.75 -.65 -.55 -.45 -.35 -.25 -.15 -.05 .05 .15 .25 .35 .45 .55 .65 .75 .85

Figure 5

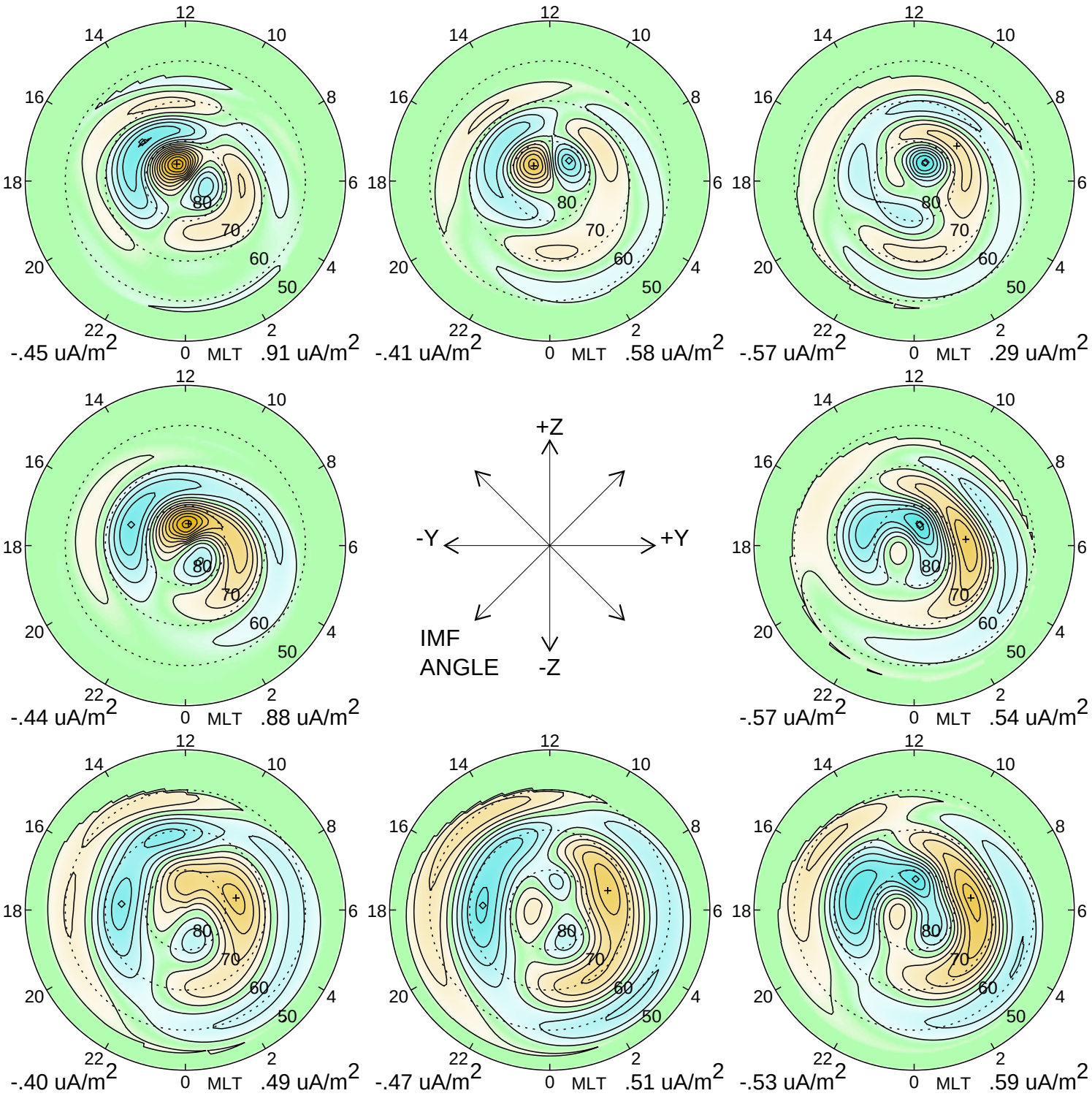
Field Aligned Current
IMF B_T= 5.0 nT V_{SW}=400. km/s N_{SW}= 5.0 /cc Tilt= 23.4^o
-.45 uA/m^2 .91 uA/m^2
-.41 uA/m^2 .58 uA/m^2
-.57 uA/m^2 .29 uA/m^2
-.44 uA/m^2 .88 uA/m^2
-.57 uA/m^2 .54 uA/m^2
-.40 uA/m^2 .49 uA/m^2
-.47 uA/m^2 .51 uA/m^2
-.53 uA/m^2 .59 uA/m^2
MLT
+Z
-Y
+Y
-Z
IMF
ANGLE
uA/m^2
-.85 -.75 -.65 -.55 -.45 -.35 -.25 -.15 -.05 .05 .15 .25 .35 .45 .55 .65 .75 .85

Figure 6

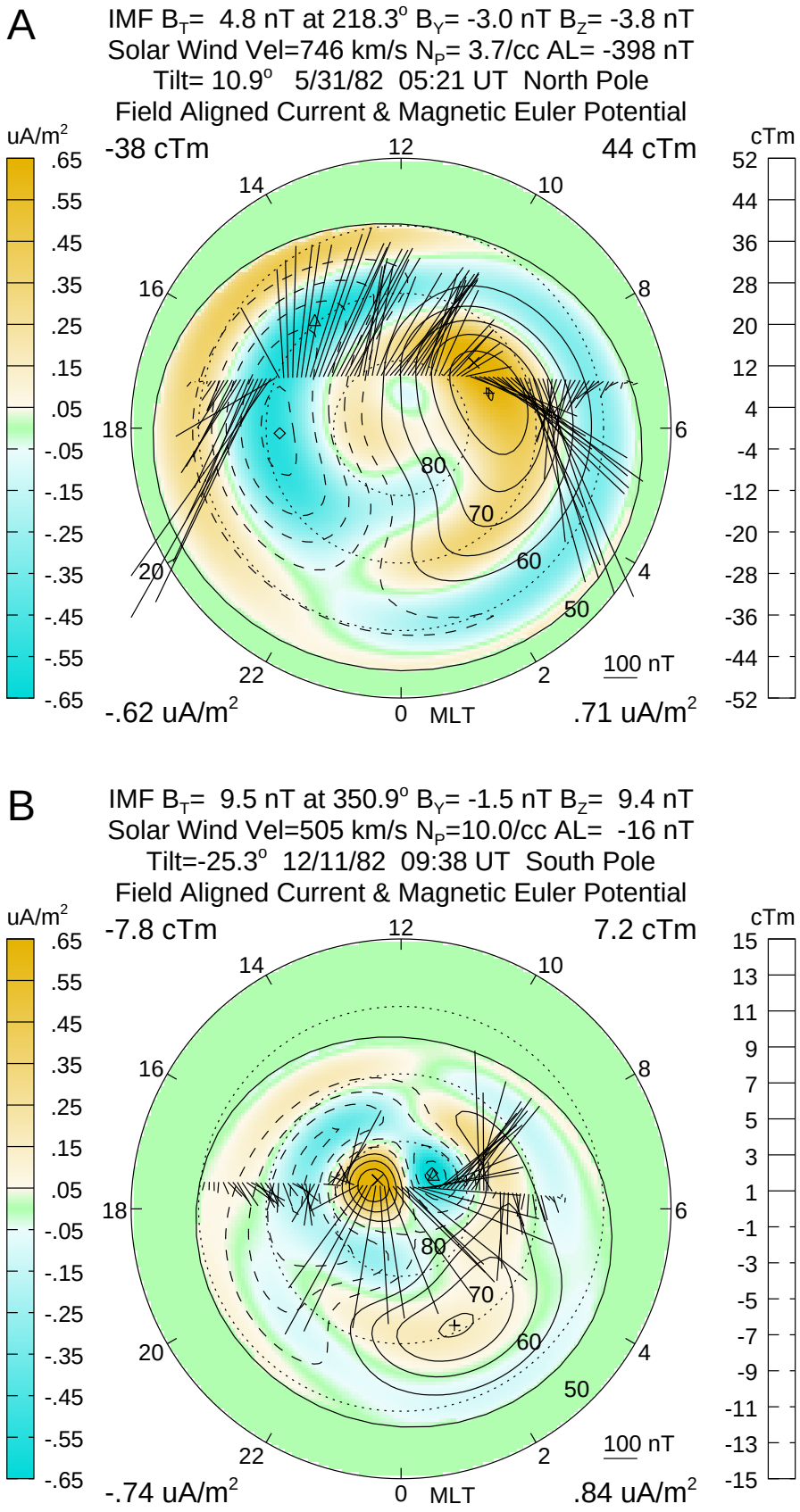
A
IMF B_T= 4.8 nT at 218.3° B_Y= -3.0 nT B_Z= -3.8 nT
Solar Wind Vel=746 km/s N_P= 3.7/cc AL= -398 nT
Tilt= 10.9° 5/31/82 05:21 UT North Pole
Field Aligned Current & Magnetic Euler Potential
uA/m²
.65
.55
.45
.35
.25
.15
.05
-.05
-.15
-.25
-.35
-.45
-.55
-.65
-38 cTm
44 cTm
cTm
52
44
36
28
20
12
4
-4
-12
-20
-28
-36
-44
-52
12
14
10
16
8
18
6
20
4
22
2
0
MLT
80
70
60
50
100 nT
-.62 uA/m²
.71 uA/m²
B
IMF B_T= 9.5 nT at 350.9° B_Y= -1.5 nT B_Z= 9.4 nT
Solar Wind Vel=505 km/s N_P=10.0/cc AL= -16 nT
Tilt=-25.3° 12/11/82 09:38 UT South Pole
Field Aligned Current & Magnetic Euler Potential
uA/m²
.65
.55
.45
.35
.25
.15
.05
-.05
-.15
-.25
-.35
-.45
-.55
-.65
-7.8 cTm
7.2 cTm
cTm
15
13
11
9
7
5
3
1
-1
-3
-5
-7
-9
-11
-13
-15
12
14
10
16
8
18
6
20
4
22
2
0
MLT
80
70
60
50
100 nT
-.74 uA/m²
.84 uA/m²

Figure 7

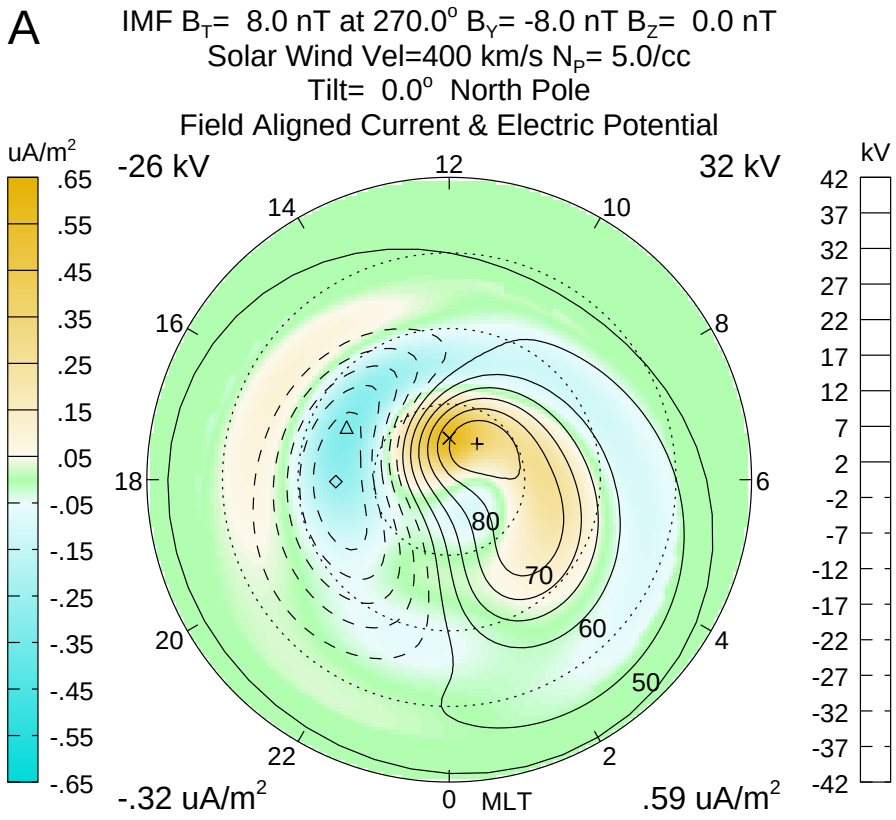
A
IMF B_T= 8.0 nT at 270.0° B_Y= -8.0 nT B_Z= 0.0 nT
Solar Wind Vel=400 km/s N_P= 5.0/cc
Tilt= 0.0° North Pole
Field Aligned Current & Electric Potential
uA/m²
.65
.55
.45
.35
.25
.15
.05
-.05
-.15
-.25
-.35
-.45
-.55
-.65
-26 kV
32 kV
kV
42
37
32
27
22
17
12
7
2
-2
-7
-12
-17
-22
-27
-32
-37
-42
12
14
10
16
8
18
6
20
4
22
2
0
MLT
80
70
60
50
-.32 uA/m²
.59 uA/m²

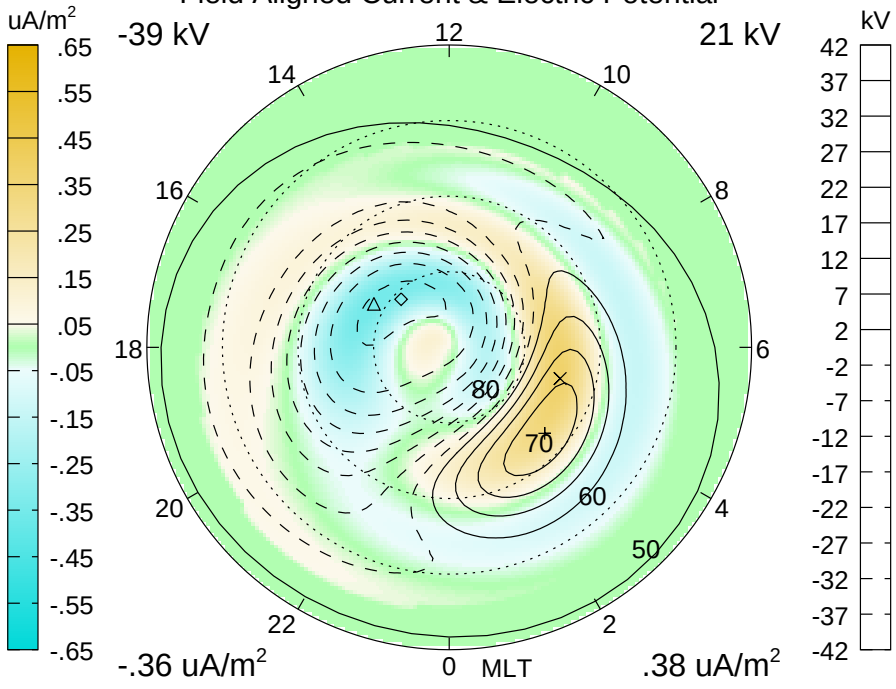
B
IMF B_T= 8.0 nT at 90.0° B_Y= 8.0 nT B_Z= 0.0 nT
Solar Wind Vel=400 km/s N_P= 5.0/cc
Tilt= 0.0° North Pole
Field Aligned Current & Electric Potential
uA/m²
.65
.55
.45
.35
.25
.15
.05
-.05
-.15
-.25
-.35
-.45
-.55
-.65
-39 kV
21 kV
kV
42
37
32
27
22
17
12
7
2
-2
-7
-12
-17
-22
-27
-32
-37
-42
12
14
10
16
8
18
6
20
4
22
2
0
MLT
80
70
60
50
-.36 uA/m²
.38 uA/m²

Figure 8

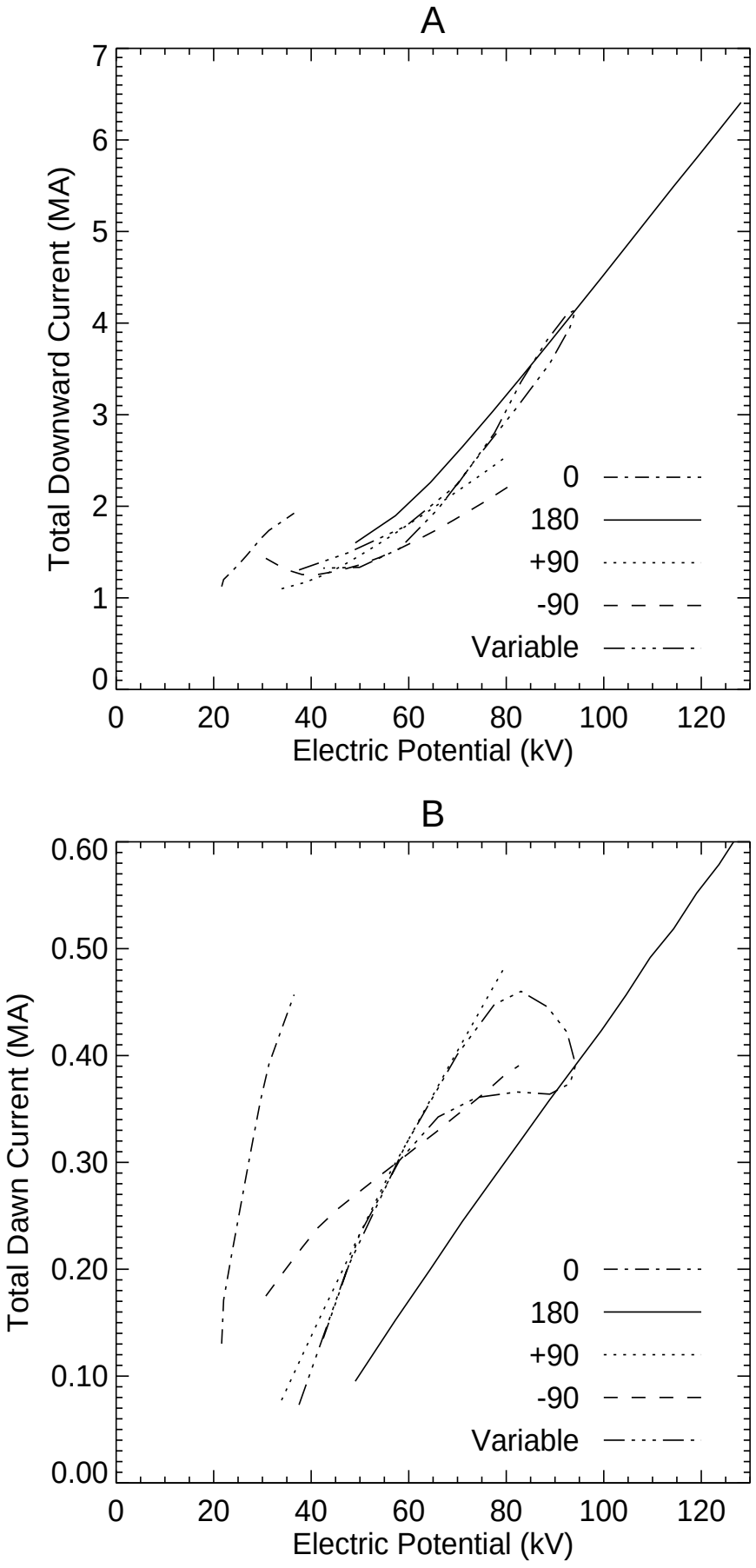
A
Total Downward Current (MA)
Electric Potential (kV)
0
180
+90
-90
Variable
B
Total Dawn Current (MA)
Electric Potential (kV)
0
180
+90
-90
Variable

Figure 9

Field Aligned Current

IMF Angle= 90.0^{o} B_T= 5.0 nT V_{SW}=400. km/s N_{SW}= 5.0 /cc Tilt= 0.0^{o}

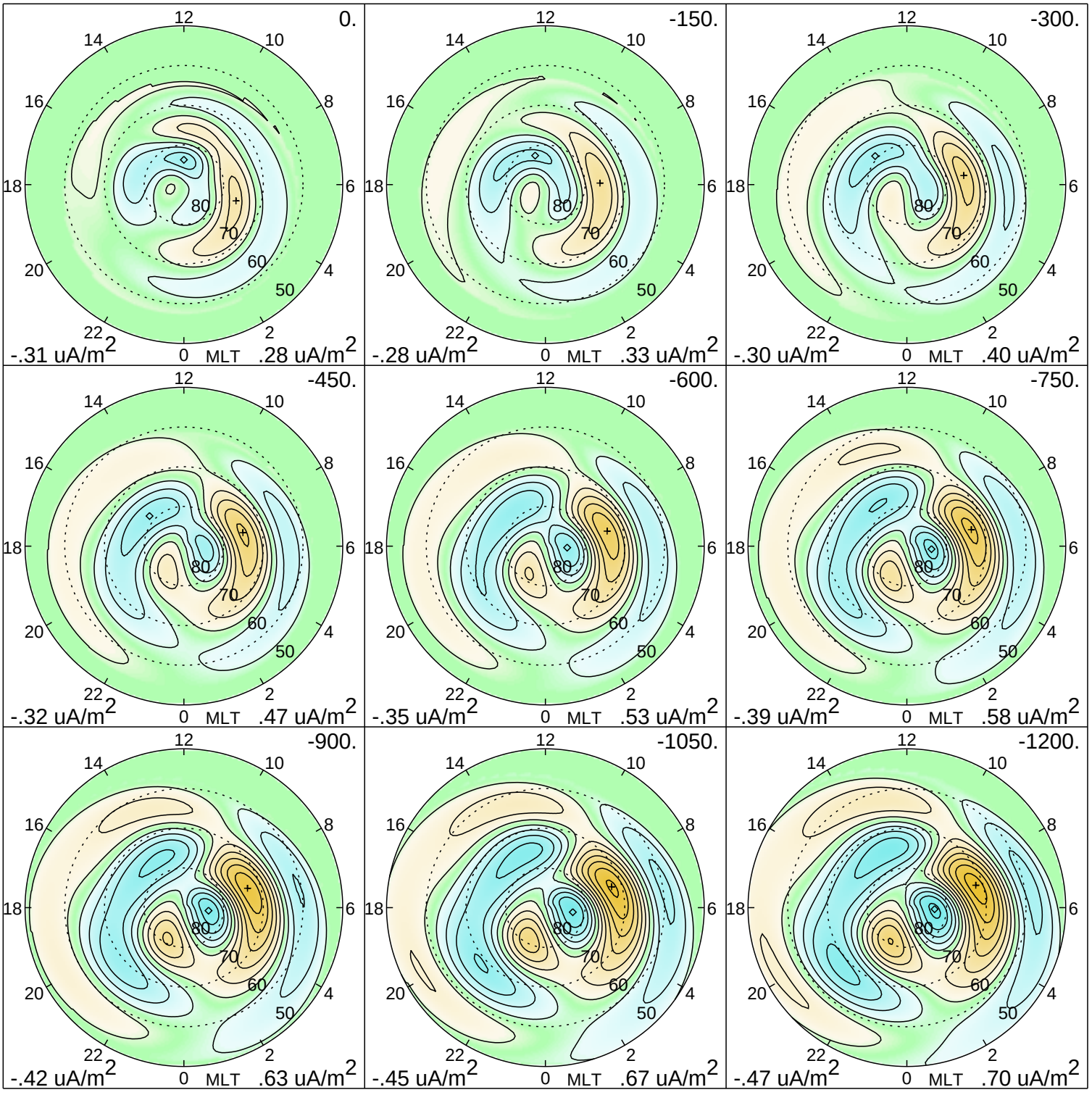

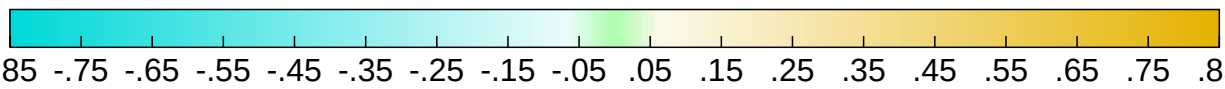

Figure 10